THE BALTIC JOURNAL
OF ROAD AND BRIDGE ENGINEERING

2012
7(2): 137–144

RAILWAY BRIDGE USING SMALL POST-TENSIONED CONCRETE BOX GIRDER

Inkyu Rhee

High-Speed Rail System Research Center, Korea Railroad Research Institute,
360-1 Woram-dong, Uiwang, Gyeonggi-Do 437-757, Republic of Korea
E-mail: rheei@krri.re.kr

Abstract. A girder depth is the critical parameter for rapid construction of bridge and clearance limitation in urban area such as high-density residential district. A standard post-tensioned I-shaped concrete girder usually demands relatively higher girder depth in order to retain sufficient moment arm between compressive and tensile fiber. To elaborate this issue, a small rectangular hollowed section can be used as a replacement of I-shaped standard girder. This small post-tensioned concrete box girder allows more flexible girder depth adjustment rather than standard I-shaped post-tensioned girder plus additional torsion resistance benefits of closed section. A 30 m long, 1.7 m high and 3.63 m wide actual small post-tensioned concrete box girder is designed. A laboratory test was performed for its static behaviors by applying 6400 kN amount of load in the form of 4-point bending test. The load-deflection curve and crack patterns at different loading stage are recorded. In addition, to extract the dynamic characteristics; natural frequency and damping ratio of this girder, several forced vibration tests using oscillator are carried out with varying operational frequency. Nonlinear finite element analysis of this 4-point bending test under monotonic static load is discussed with the aid of concrete damaged plasticity using ABAQUS program. Finally, a series of modal dynamic analyses of different span length and girder depth of small post-tensioned girder bridge is performed in order to validate the applicability to railway bridge and compared to the UIC design criteria in the form of time dependent dynamic responses such as deflection, acceleration and end rotation.

Keywords: small box girder, full-scaled test, vibration test, concrete plasticity, modal dynamics, railway bridge.

1. Introduction

Since pre-stressed concrete beam has been applied in various civil infrastructures starting from 1960s, many sorts of pre-stressed concrete (PSC) girder have been developed and applied as a main flexural member for highway/railroad bridges around the world. The main advantages of this PSC girder is an ease of factory-manufacture and fabrication resulting into rapid construction, flexible choice of girder depth by adjusting initial jacking force aside from other advantages and disadvantages. These aspects are quite effective and appropriate in needs of rapid and efficient construction for urban site. In case of railroad bridges, numerous type of prestressed-like girder such as Pre-flex girder (Portela *et al.* 2011), steel-composite PSC girder (Rhee *et al.* 2010), post-tensioned girder with re-adjustable jacking force, PSC girder with enhanced compression steel panel are being developed in worldwide.

Some of these girders are already used for highway/railroad bridges but some of those are not and still are being tested in order to balance the paradox between structural safety and serviceability issues (Ju *et al.* 2003, 2008; Rhee *et al.* 2010). The basic load bearing capacity is primary aspect for PSC girder design associated with concrete compressive strength, tendon/strands strength, jacking force with a specific limitation of clearance. Sometimes, bridge designer reluctantly selects a smaller cross-section with relatively large jacking force in order to meet this construction limit. However, it may reproduce a resonance in a slender bridge superstructure with high longitudinal strength by car/train travel-induced forced vibration. Therefore, these two main aspects must be checked before applying the designed PSC girder to real construction work.

In this paper, a small post-tensioned box girder bridge is proposed in order to achieve rapid construction for urban site and cost-effective bridge especially for medium long range of span, 25–40 m. The small post-tensioned box girder has identical cross-sectional shape basically compared to a typical single or double box girder as depicted in Fig. 1. Nevertheless this less-particular feature, the

ISSN 1822-427X print / ISSN 1822-4288 online
doi: 10.3846/bjrbe.2012.19
http://www.bjrbe.vgtu.lt

parallel array of these small miniature box girders guarantees that an available bridge span can be extended further. This small box girder still has better resistance to torsion, which is particularly of benefit if the bridge deck is curved in plan. Since the traditional single box girder is required a cast-in-place type of construction, a false works (including formwork/scaffolds) are needed so that construction cost is normally expensive. In contrast, a small version of box girder can be pre-cast in vicinity of construction site and fabricated in easy and fast manner as typical pre-cast concrete girder manufacture and fabrication.

In order to validate the performance of this small box girder bridge, the two main issues are investigated in experiment for both structural safety and serviceability. The former is achieved by 4-point bending test and the latter is by forced vibration test and time-history analyses. The 4-point bending test is followed to evaluate the structural behaviors under a monotonic force/displacement control up to 6400 kN. The forced vibration test is performed using inertial mass oscillator for measuring the natural frequency (prominent frequency) and damping ratio in elastic range of deformation. Finally a series of the modal dynamic analysis of 30 m long 3-small box girder bridge is performed under the different level of train speed up to 320 km/h. The train load specification is based on KTX (Korean Train eXpress) which is identical to TGV in France.

2. Experimental tests on 30 m long post-tensioned concrete box girder

2.1. Static test

Experimental investigations for overall railway bridge were done by a few researchers (Zhou *et al.* 2004; Xia *et al.* 2004; Liu *et al.* 2009) under high speed train loads. In this paper, a single full-scaled girder as a bridge member was selected for failure test. The test specimen is 3.63 m wide, 2.0 m depth and 30 m long small pre-stressed box girder as shown in Fig. 1. The 7-wired prestressed concrete strands are installed for applying preloading the amount of 1041 MPa. The compressive strength of concrete is $f_c^{'}$ = 45 MPa and the elastic modulus of concrete is E_c = 29 837 MPa with specific weight, γ_c = 24.5 kN/m^3. The PC tendon is basically used for low-relaxation steel with yield strength, f_{PY} = 1600 MPa. The elastic modulus of steel is 210 000 MPa and the specific weight γ_s is 78.0 kN/m^3. This particular girder specimen has been designed for the one of identical dimension of 3-girder railway bridges under Korean LS-22 loads (equivalent with UIC loads).

A 4-point bending test is performed in order to explore the failure patterns and its flexural beam capacity such as cracking load, initial global stiffness and secondary global stiffness after dominant crack distributions in test specimen. Fig. 1a represents the test apparatus with two vertical actuators which can exhibit nearly 6400 kN compressive loads in sum in the form of typical hydraulic oil pressure. The gap between actuator-to-actuator is 5.0 m which means this girder specimen could be experienced

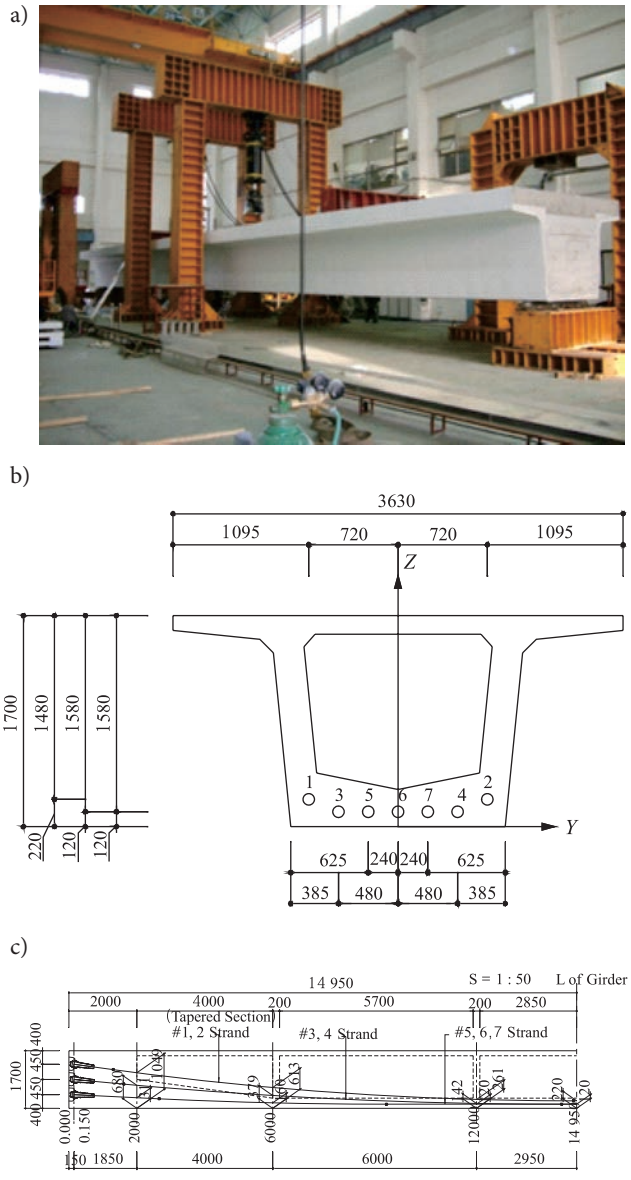

Fig. 1. Test specimen: 30 m long, 3.63 m wide and 2.0 m high small post-tensioned concrete box girder, in mm

with narrow shear-free zone in the center region of girder length. A total of 24 concrete gauges, 30 steel strain gauges are attached in three different girder sections, L/4, L/2 and 3L/4. These gauges transmit mainly the concrete edge fiber cracking in tension (lower plane) and tension/shear (web) region below the neutral axis of the girder and steel strain information at the level of longitudinal reinforcements. In addition, the compressive concrete strain and steel strain are also traced in the form of strain gauges. The 3 of LVDTs are set underneath the two quarter points and the center point of girder length in order to measure the vertical deflections. 2 rosette strain gauges are attached in the vicinity of the end supports.

A force control with 2 actuators is applied initially to reach fast on the point of the cracking load (3254 kN) up to 3400 kN with 10–50 kN/min loading speeds. Once the cracking load has been reached and applied the load

is released to initial load-free stage and reloaded repeatedly but with displacement control methods to prohibit the abrupt brittle failure of the specimen girder (0.1–0.15 mm/min). After the reloading sequence, the total loads are applied up to 6400 kN which is the full loading capacity of test actuators and finished at the load stage of 6400 kN. The apparent failure is not developed fully yet at the stage of 6400 kN though. Fig. 2 illustrates the crack patterns at the 3 different loading stages: a) 0–4400 kN, b) 4400–5600 kN and c) 5600–6400 kN. Since the cracking load is 3254 kN, the loading stage (Fig. 2a) exhibits mainly flexural crack in the lower-center of the girder. In loading stage (Fig. 2b) the flexural cracking is extended more vertically in the center region and diagonal tension cracks are developed as the beam curvature is increased. A similar crack patterns but severe case is dominant also at the final loading stage, (Fig. 3c) 6400 kN.

2.2. Forced vibration test for dynamic characteristics extraction

The lower natural frequencies and damping ratio under free vibration are essential to model the railway bridges in computer simulation (Bayraktar *et al.* 2009; Ju *et al.* 2008; Rhee *et al.* 2010). Since the 3-girder railway bridge under high-speed train moving loads is concerned in this paper, one can extract this basic strain energy tuning parameters such as triple products of the min eigenvalue (natural frequency) with associated eigenmode which is the 1st order bending motion and the frictional dynamic energy loss can be normalized with the term of damping ratio in the assumption of damage-free condition of the test specimen. To this end, the artificial forced vibration test is performed prior to static loading test (4-point bending test) in elastic load range with aids of un-symmetric inertial mass oscillator on the top of the girder by anchoring mechanically with bolts.

Fig. 3a shows the typical oscillator and impact hammer in order to capture the natural frequency and damping ratio of the girder. The accelerometers are chemically bonded on the top of the girder at the points of L/4, L/2 and 3L/4. The oscillator is sweeping up the operating frequency from 0~10 Hz. During the sweep-up control, the resonance behavior of recorded acceleration history can be exhibit due to the overlap with natural frequency of the girder and the operating frequency of the oscillator. Fig. 3b indicates the max vertical acceleration values corresponding to the different operating frequencies. In the vicinity of 4.5 Hz point, the vertical acceleration history exhibit abruptly large oscillation as compared to other histories at different frequency band. One can recognize the natural frequency of the girder as a resonant frequency which is 4.52 Hz. The lower graph of Fig. 3b shows the typical eigenmode (1st mode of flexure) by bridging the max acceleration values from the different points, L/4, L/2 and 3L/4. This can be also found with impact test with electrical hammer as shown in Fig. 3c. The relatively lesser impact energy gives small measured acceleration level but indicates similar natural frequency after a low pass filtering. After a forced vibration using oscillator is cancelled, a free vibration is dominant in the girder so that one can regularize the peak decrements with logarithmic function as known as a damping ratio, $\zeta(\%) = \left(\frac{1}{2\pi n}\right)\ln\left(\frac{a_0}{a_n}\right)$. Since a total of 15 forced vibration tests are performed with different operating frequency of the oscillator, one can extract the average damping ratio out of 15 different measured damping ratios which is 0.8%.

3. Computer simulations

The numerical simulation efforts with nonlinear material laws in RC/PSC girder are worthwhile to examine

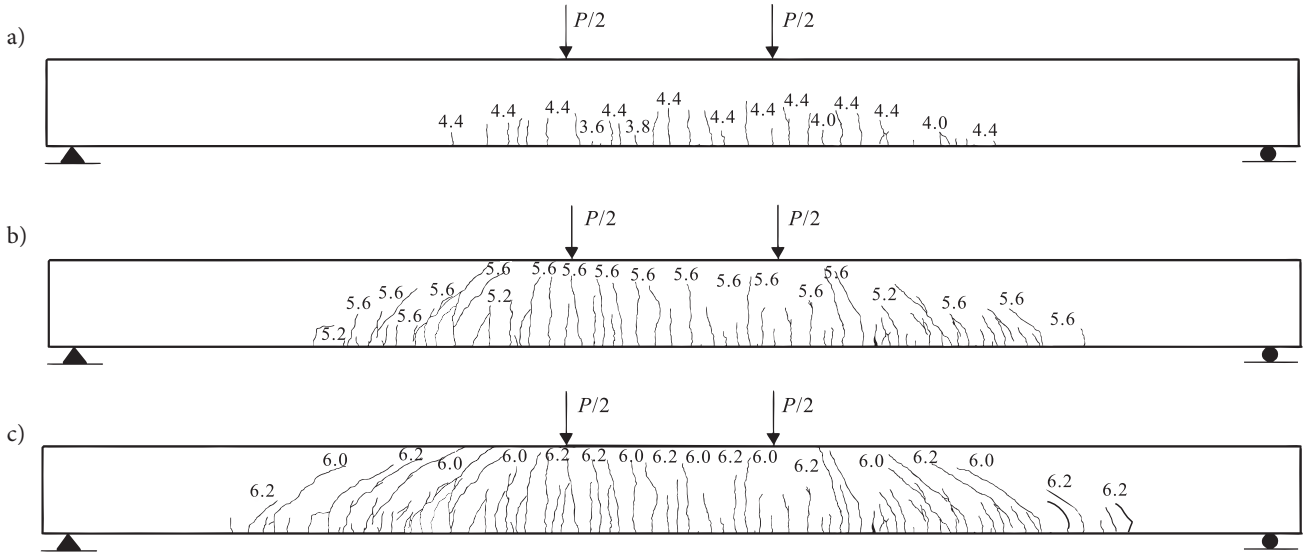

Fig. 2. Crack patterns at different loading stages: a – 0–4400 kN; b – 4400–5600 kN; c – 5600–6400 kN (Crack load: 3254 kN).
Note: unit is MN-scale inside the girders

thorough life of test specimen and allow exploring fine local/global behaviours (Rhee *et al.* 2006; Basche *et al.* 2007; Gribniak *et al.* 2010). The compressive tests for standard concrete cylinders are tested to measure the compressive strength deviation compared to the designed strength which is 45.0 MPa. An elastic modulus of concrete cylinder is averaged among a few compressive test results. Fig. 4 shows the mesh layout of finite element discretization using ABAQUS. A thin shell element is basically used for constructing the geometry of U-shaped web and slab in 3D. Longitudinal reinforcements and pre-stressing tendons are modeled using a beam element. The material nonlinearities are imposed in concrete shell parts with strain damage (softening) law using Lee & Fenves model (Lee, Fenves 1998). A bilinear hardening law is adopted for longitudinal reinforcements and tendons respectively. A displacement control is used for applying the loads to the model specimen. Tension damages of concrete elements are basically traced in the form of scalar damage variable from 0 to 1. While the undamaged situation indicates 0, a progressive damage can be measured by elevating secant damage as a tensile cracks as shown in Fig. 4a.

Initially, a few vertical tension cracks are developed at the lower faces in the center of girder length and as the load level is increased, the diagonal tensile cracking is developed and is propagated toward end supports. Alternative representation of crack distribution is the plot of effective plastic strains with vector formats in Fig. 4b. The orthogonal direction in Fig. 4b would be a cracking direction while the linear vector line and length indicates the tensile straining in its planar direction.

Finally, the global force (reaction) and center deflection curve is basically compared with experimental evidence and computer simulation results in Fig. 5a. The center deflection and the quarter deflection are basically traced and are fairly close to each other. The inflection points and post-peak hardening slopes are slightly different from each other. It means that the a little bit different bending strength and crack distributions/localizations (reinforcement/tendon effects) between experimental configuration and numerical simulation. This slight differences can be produced in experimental/numerical biases such as inhomogeneous media, geometrical imperfections and boundary conditions (loading platens, rollers) and vice versa. One can find fairly close result of global behaviors of the specimen girder in 4-point bending test. Fig. 5b illustrates the migration of neutral axis when the girder is under an applied load from 0 to 6400 kN. In the meantime, the material level of stress/strain relations is recorded as a vehicle of local deformations.

Fig. 5c shows the longitudinal stress/strain relations at the level of 0, H/2, H which are a tension edge, a half depth of the girder and a compression edge respectively at the quarter section of the girder. In a similar manner, Fig. 5d depicts the longitudinal stress/strain plot at the central section of the girder. While the quarter section has experienced the dominant elastic behaviors yet in compression, a slight slope variation indicates the presence of flexural tensile cracks in the vicinity of the quarter section

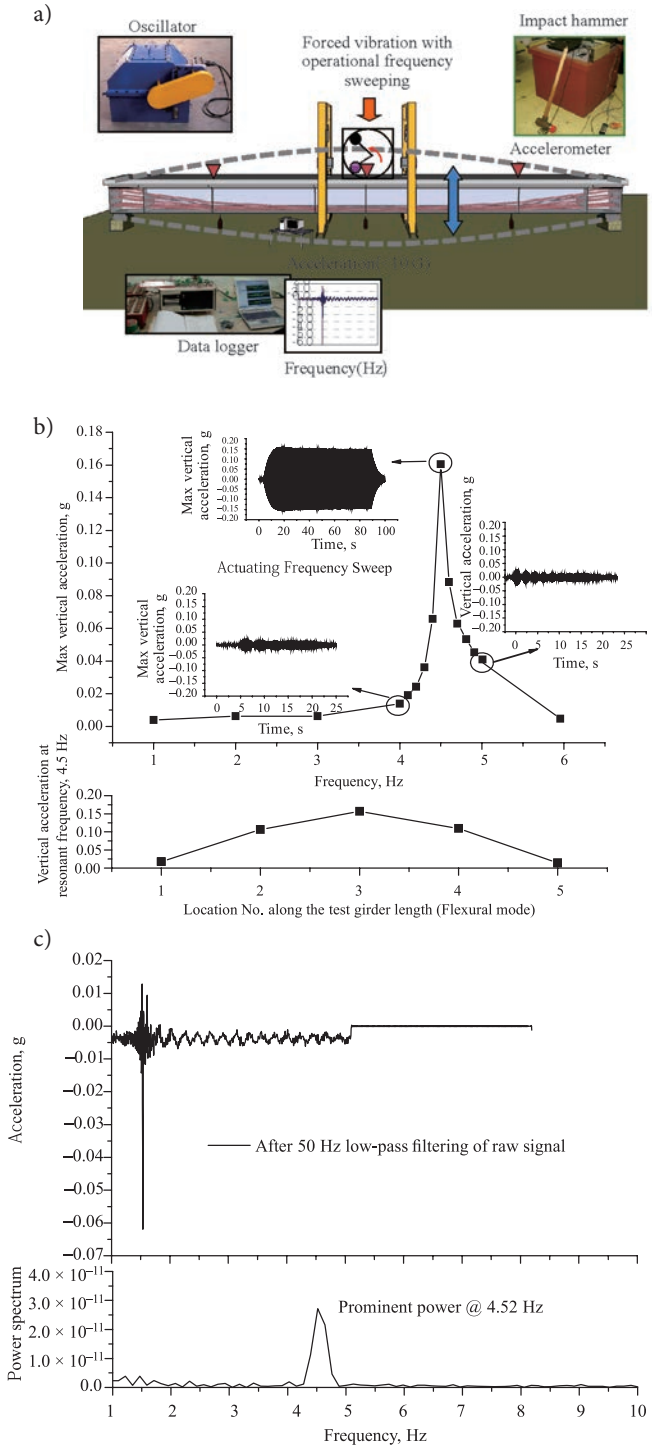

Fig. 3. Measurement of natural frequency and damping ratio: a – forced vibration test with inertial oscillator/impact hammer; b – natural frequency extraction (by oscillator); c – natural frequency extraction (by impact hammer)

(L/4 = 7.5 m). This can be also found in the crack map in Fig. 2.

In contrast, while the compression stress/strain is still close to linear in experimental observation, the numerical result has a premature degradation in compression compared to the experiment. As a consequence of this premature compressive degradation, the tensile stress/strain

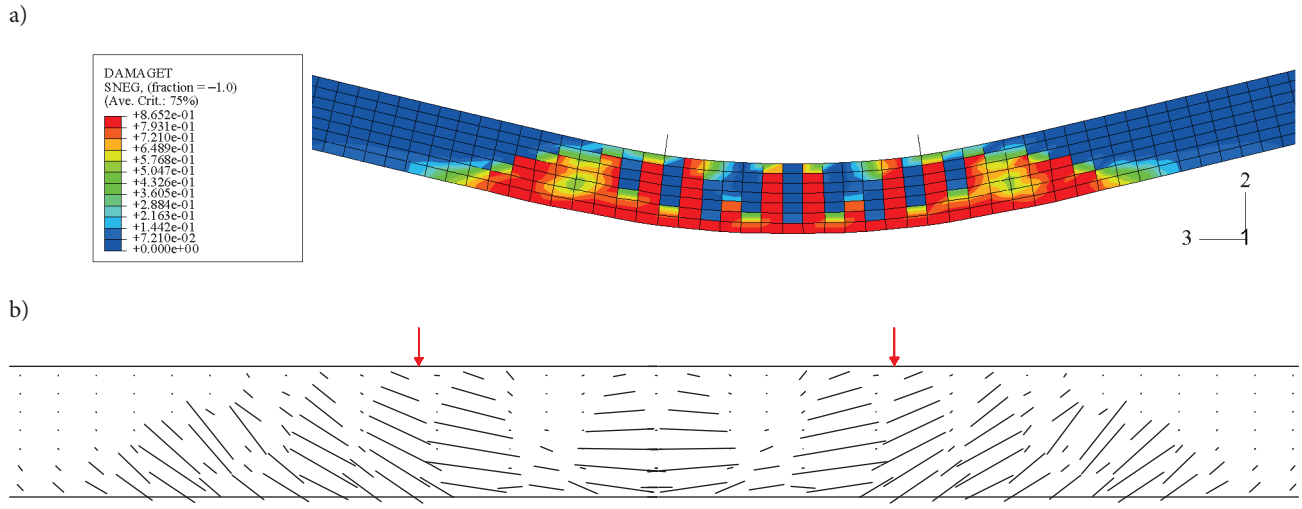

Fig. 4. Computer simulation: a – vertical/diagonal tension cracks contour plot in terms of tension damage variable: bound (0:undamaged–1:fully separated); b – vector plots for effective plastic strain

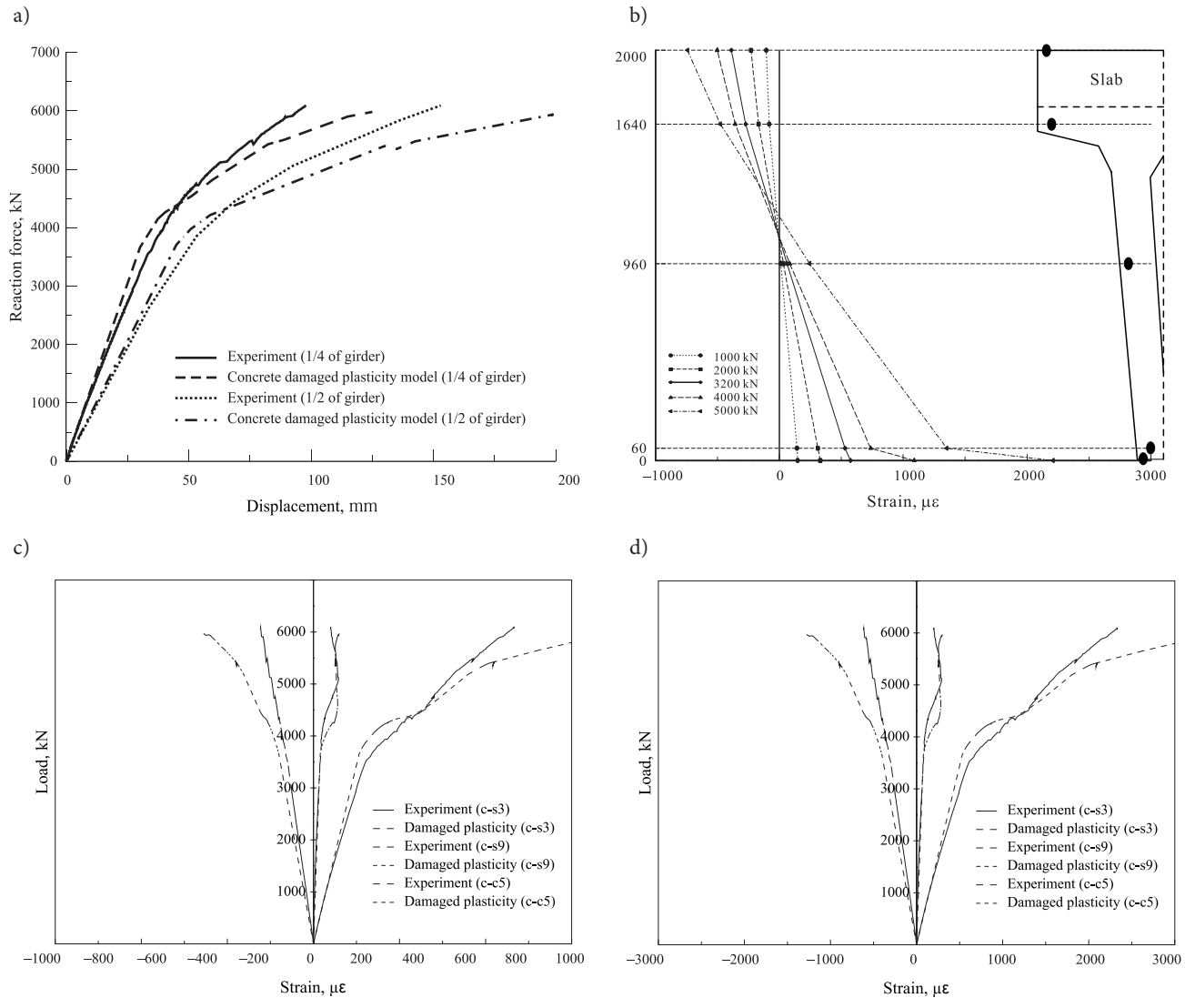

Fig. 5. Comparisons: a – applied load-central deflection curve at the central and the quarter sections: experiment vs. computer simulation; b – neutral axis migration due to progressive tension damages by increasing applied load, Longitudinal stress/strain curve at the level of the top, the center and the bottom point of the girder depth: cross-sections at c – L/4 and d – L/2

relation from numerical simulation exhibits relatively lower post-peak slope. Regarding this phenomenon, diagonal tensile cracks nearby the quarter section is getting severely localized and reaches the compression fiber of the girder as found in Fig. 4. The narrow band of compression zone is getting diminished fast so that the equilibrium between tension/compression in the cross-section is easily diverged after the load stage of 6400 kN. In order to trace the ultimate failure pattern, a sophisticate constitutive law of concrete and tendon could be expected.

4. Modal dynamic analysis for railroad bridge

In previous sections, the member test for flexural capacity and crack patterns in conjunction with computer simulation with material nonlinearities is discussed. The dynamic behaviors of a real railway bridge are now examined on the purpose of typical design process under the guidance of *UIC 774-1R:1984* criteria and Tanabe *et al.* (1987) for stability and serviceability. The Korean Train express is used for moving train load as illustrated in Fig. 6a. Fig. 6b illustrates the 3-girdered railway bridge example with 30 m long spanned, simply supported and doubly-laned. Since the flexural test of single girder has been done already in the section 2–3 earlier in the form of static and dynamic performances, The same material properties of concrete, steel and tendons in static manner and the measured dynamic property such as damping ratio of the single girder are used for modal dynamic analysis under moving train loads. The 0.8% of damping ratio is for single girder. Probably the fabrication of 3-girdered bridge exhibits higher damping ratio compared to the single girder.

The ballast, rail and concrete slab are involved to enhance stiffness and mass of bridge decks. The fundamental modes are extracted as 4.0 Hz. The moving train (Korea Train eXpress) speeds bounds from 0–320 km/h in real service life. This moving load is applied on singly-laned rail edge in order to reproduce worst bridge responses as comparing to doubly-laned load scenario. A total of 32 different modal analyses are performed at every 10 km/h step increments. A series of vertical displacement/acceleration, end rotation histories are extracted. The two specific train speeds of 130 km/h and 260 km/h are shown to identifying the max responses at critical resonance reproduced by a speed variable and a wheel-beating distance (wheel-to-wheel distances). One can distinguish the critical KTX speed in the vicinity of 260 km/h zone in this 30 m long 3-girdered bridge.

In parallel, Yang *et al.* (1997), Frỳba (2001) proposed the estimated critical speed of train by simple formula by multiplying two main variables; (a) fundamental natural frequency of a bridge, (b) effective beating interval(wheel-to-wheel distance). It also gives 269 km/h as the critical speed for possible resonance phenomenon. Vertical displacement and end rotation footprint regarding the envelops of the max values are depicted in Fig. 7 along the full speed spectrum from 0–320 km/h. Two prominent peaks are recognizable which are at the speed of 130 km/h and 260 km/h. The latter is known as primary critical speed for resonance and the former is secondary critical speed. Table 1 shows the main responses of numerical simulations in order to estimate the possibility of inclusion in actual service railroad route in the form of max dynamic response comparison.

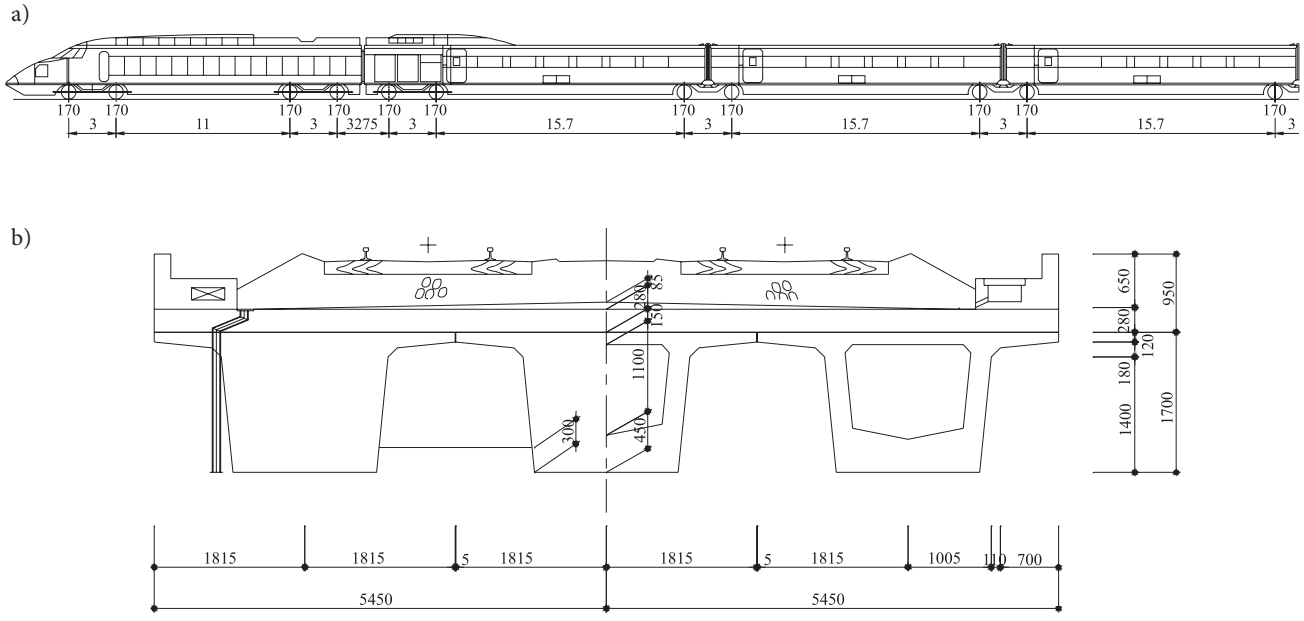

Fig. 6. Railway application: a – Korean Train eXpress (KTX) wheel loads, wheel-to-wheel distance (unit: kN, m), b – railway bridge model with slab & ballast: 30 m long span, doubly-laned rail system (unit: mm)

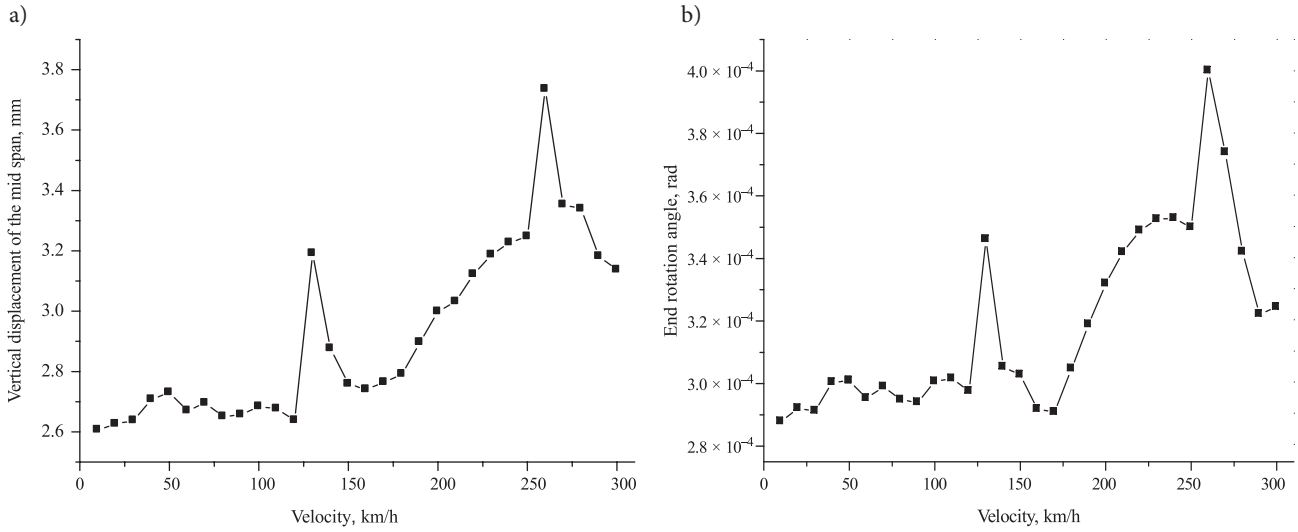

Fig. 7. Model bridge responses with the different train speed spectrum: a – vertical displacement; b – end rotation

Table 1. Summary of dynamic responses of simply supported small boxed PSC girder bridge under KTX (TGV) vehicle loading

Categories	UIC/Korean Design Codes	30 m long (3-girders)	35 m long (4-girders)
Natural frequency	a) 30 m L: 3.15–7.44 Hz b) 35 m L: 2.87–6.63 Hz	4.00	4.28
Max vertical displacement @ center	18.8–25 mm	3.74	5.08
Max vertical acceleration @ center	0.35 g w/ ballast	0.09	0.27
End rotation of superstructure	$5.0' \times 10^{-4}$ rad	4.0×10^{-4}	4.7×10^{-4}
End relative vertical displacement	2.0 mm	0.174	0.215
Twist of superstructure	0.4 mm/m	0.129	0.058

5. Conclusion

The 30.0 m long, 3.63 m wide and 2.0 m high small box-shaped PSC girder is proposed as an alternative of current standard I-shaped PSC girder which is little adjustable against clearance limitation or excessively designed current single box PSC girder in railroad bridges in Korea.

1. This real-scaled single girder is tested and analyzed with the aid of static and dynamic laboratory tests in the form of 4-point bending test and oscillation test respectively. The main observations drawn from these tests are the load bearing capacities and basic dynamic properties such as force-displacement relation, flexural stress/strain relation, natural frequency and damping ratio of the test girder etc. Further case studies with computer simulations are performed as a material nonlinear analysis under monotonic loading in order to cross-examine the failure pattern of the girder with experimental evidences.

2. Finally, experimental measures of natural frequency and damping ratio are used for calibrating the modal dynamic test of the series of different girder amounts and span length. Although all items related with railroad bridge stability and serviceability are met with UIC and Korean design code both, 30–35 m long of test span with this proposed girder under actual service railroad route should be monitored in a long term basis with some of durability/fatigue issues exposed in real harsh environments in the future.

Acknowledgement

The author wishes to acknowledge partial support under the Grant No. CP07013 of Korea Railroad Research Institute from *EnE Construction Co*, *Korea Development Co*., *Shinsung Engineering Co*. and *KG Engineering Co*. of Korea. The opinions expressed in this paper do not necessarily reflect those of the sponsors.

References

Basche, H. D.; Rhee, I.; Willam, K. J.; Shing, P. B. 2007. Analysis of Shear Capacity of Lightweight Concrete Beams, *Engineering Fracture Mechanics* 74(1–2): 179–193. http://dx.doi.org/10.1016/j.engfracmech.2006.01.012

Bayraktar, A.; Birinci, F.; Altunışık, A. C.; Türker, T.; Sevim, B. 2009. Finite Element Model Updating of Senyuva Historical Arch Bridge Using Ambient Vibration Tests, *The Baltic Journal of Road and Bridge Engineering* 4(4): 177–185. http://dx.doi.org/10.3846/1822-427X.2009.4.177-185

Frỳba, L. 2001. A Rough Assessment of Railway Bridges for High Speed Trains, *Engineering Structures* 23(5): 548–556. http://dx.doi.org/10.1016/S0141-0296(00)00057-2.

Gribniak, V.; Kaklauskas, G.; Idnurm, S.; Bačinskas, D. 2010. Finite Element Mesh Size Effect on Deformation Predictions of Reinforced Concrete Bridge Girder, *The Baltic Journal of Road and Bridge Engineering* 5(1): 19–27. http://dx.doi.org/10.3846/bjrbe.2010.03

Ju, S. H.; Lin, H. T. 2003. Resonance Characteristics of High-speed Trains Passing Simply Supported Bridges, *Journal of Sound and Vibration* 267(5): 1127–1141. http://dx.doi.org/10.1016/S0022-460X(02)01463-3

Ju, S. H.; Lin, H. T.; Huang, J.-Y. 2008. Dominant Frequencies of Train-Induced Vibrations, *Journal of Sound and Vibration* 319(1–2): 247–259. http://dx.doi.org/10.1016/j.jsv.2008.05.029 .

Lee, J.; Fenves, G. 1998. A Plastic-Damage Concrete Model for Earthquake Analysis of Dams, *Earthquake Engineering and Structural Dynamics* 27(9): 937–956. http://dx.doi.org/10.1002/(SICI)1096-9845(199809)

Liu, K.; Reynders, E.; Roeck, G. D.; Lombaert, G. 2009. Experimental and Numerical Analysis of a Composite Bridge for High-Speed Trains, *Journal of Sound and Vibration* 320(1–2): 201–220. http://dx.doi.org/10.1016/j.jsv.2008.07.010

Portela, G.; Barajas, U.; Albarran-Garcia, J. 2011. *Analysis and Load Rating of Pre-Flex Composite Beams.* US Army Corps of Engineers, Engineer Research and Development Center], Geotechnical and Structures Laboratory. 79 p.

Rhee, I.; Kim, L. H.; Kim, H. Y.; Lee, J. B. 2010. Dynamic Behaviors of Skewed Bridge with PSC Girders Wrapped by Steel Plate, *International Journal of Railway* 3(3): 83–89.

Rhee, I.; Lee, H. U.; Lee, J. S.; Kim, W. 2006. Failure Analysis of Reinforced Concrete Bridge Column Using Cohesive and Adhesive Interfaces, *Key Engineering Materials* 321–323: 716–719. http://dx.doi.org/doi:10.4028/www.scientific.net/KEM.321-323.716

Tanabe, M.; Yamada, Y. 1987. Modal Method for Interaction of Train and Bridge, *Computers & Structures* 27(1): 119–127. http://dx.doi.org/10.1016/0045-7949(87)90187-8

Xia, H.; Zhang, N.; Gao, R. 2004. Experimental Analysis of Railway Bridge under High-Speed Trains, *Journal of Sound and Vibration* 282(1–2): 517–528. http://dx.doi.org/10.1016/j.jsv.2004.04.033

Yang, Y. B.; Yau, J. D.; Hsu, L. C. 1997. Vibration of Simple Beams Due to Trains Moving at High Speeds, *Engineering Structures* 19(11): 936–944. http://dx.doi.org/10.1016/S0141-0296(97)00001-1

Zhou, S.; Rizos, D. C.; Petrou, M. F. 2004. Effects of Superstructure Flexibility on Strength of Reinforced Concrete Bridge Decks, *Computers* & *Structures* 82(1): 13–23. http://dx.doi.org/10.1016/j.compstruc.2003.08.009

Received 26 August 2010; accepted 2 November 2011